

Molecular-dynamics simulation of tweed structure and the ω phase in Ni-Al

C. S. Becquart, P. C. Clapp, and J. A. Rifkin

Center for Materials Simulation, Institute of Materials Science, University of Connecticut, Storrs, Connecticut 06269-3136

(Received 16 December 1992)

Using computer molecular dynamics (CMD) we have studied the occurrence of tweed structure and of the ω phase in $\text{Ni}_{62.5}\text{Al}_{37.5}$. Tweed is a mottled structure that is observed prior to transformations such as martensitic transformations. In some cases, it has been found to accompany ω -phase formation. The characteristic features of tweed have been simulated. To achieve the 62.5–37.5 composition we started with a 50%-50% stoichiometry in which some aluminum atoms were replaced by nickel. Two different lattices were used: one where the nickel atoms were distributed at random on the aluminum sublattice (referred to as the disordered $B2$ array) and one where they were arranged in an ordered manner (ordered supercell bcc). To describe the forces that interact between the atoms an embedded-atom method was chosen with an interatomic potential derived by Voter and Chen [1] [in *Characterization of Defects in Materials*, edited by R. W. Siegal, J. R. Weertman, and R. Sinclair, MRS Symposia Proceedings No. 82 (Materials Research Society, Pittsburgh, 1987)], which has been designed to fit some properties of Ni_3Al , and some of NiAl , while maintaining good behavior for compositions in between. In the case of the disordered $B2$ array, diffuse streakings were observed in the diffraction patterns of the structures obtained from the CMD simulations, mainly along the $\langle 110 \rangle^*$ directions but some also along the $\langle 112 \rangle^*$ direction. The $\langle 112 \rangle^*$ streaking is usually associated with the formation of the ω phase. However, with the ordered array, virtually no streaking appeared, strongly suggesting that heterogeneous defects (such as compositional disorder) are necessary to induce both tweed structure and the ω phase. The main type of streaking is typically seen on diffraction patterns of materials displaying tweed. By plotting the positions of the atoms and their displacements after the CMD runs we also noticed $\langle 110 \rangle \{100\}$ shears, again in the disordered lattice. The influence of temperature on tweed, and its evolution versus time was then studied. It was found that tweed decreases in intensity when the temperature increases as is also observed experimentally. It was also found that tweed has two different regimes: a static regime at low temperature and a dynamic regime at high temperature, in agreement with inelastic-scattering experiments.

I. INTRODUCTION

One of the outstanding problems in the field of phase transformations is the origin of the tweed microstructure that appears upon cooling prior to many transformations (for example, spinodal decomposition, ordering, or martensitic transformations) and especially those involving a cubic-to-tetragonal symmetry change. Since its characterization by Tanner¹ in 1966 in Cu-Be alloys during the formation of Guinier-Preston (GP) zones, tweed has been widely studied because of its possible precursor relationships to martensitic transformations.

Tweed draws its name from the bright-field transmission electron microscope images which resemble tweed fabrics. In the diffraction mode, tweed is characterized by diffuse streaking along the $\langle 1+h, 1-h, 0 \rangle^*$ directions at the $1-10^*$ spots with extinctions characteristic of a $\langle 110 \rangle$ shear. Its manifestation starts well above the transition temperature, and the pattern becomes more and more pronounced as the temperature decreases.² Along with the appearance of tweed, lattice softening is often observed; i.e., the elastic constant $C' = (C_{11} - C_{12})/2$ decreases when approaching the transition temperature.³ Anomalies such as an unusual dip at some frequency in the phonon dispersion curves or satellite peaks flanking the Bragg peak for the inelastic-neutron-scattering spectra⁴ have also been reported in some cases. Some au-

thors⁵ report the concurrent occurrence of other streaks along the $\langle 1-32 \rangle^*$ and $\langle 112 \rangle^*$ directions, but those streaks are not as intense as the $\langle 110 \rangle^*$ streaks. (The asterisk represents a quantity in reciprocal space.)

There are two main theories to explain the origin of tweed. The first one states that tweed is a heterogeneous phenomenon due to defects with a tetragonal strain field;^{1,5} it is therefore a static theory. The second theory explains the nucleation of tweed as a homogeneous event associated with the anharmonicity of the lattice arising from the softening of the lattice prior to the transformation;^{4,6-8} it is thus a dynamic theory.

Both theories have their partisans. The purpose of the present study was to simulate tweed in a computer and study it on the atomic scale in order to test both theories. We strove to fit our simulation as closely as possible to a real system. $\text{Ni}_{62.5}\text{Al}_{37.5}$ was chosen because this alloy has a martensitic transformation around 200 K with evidence of a very strong tweed pattern prior to the transformation. It is for these reasons widely studied, and many experimental results are available for comparison.

II. CONDITIONS OF THE COMPUTER SIMULATIONS

Although the resolution of electron microscopes has been getting progressively sharper, it is still not possible

to observe the individual dynamic behavior of atoms or molecules. However, with computer simulations it is possible to do so, to get results much faster than with experiments, and to vary parameters such as the temperature, the size of the array, etc., in a convenient way. In the computer molecular-dynamics (CMD) method used, at each time step the computer calculates the force for every particle and predicts a new set of positions and velocities for the next step. This process is repeated many times to obtain the evolution of the system. One step in our simulations corresponds to 0.03 ps. To avoid having free surfaces in the simulated array, periodic boundary conditions were used.

The force acting upon each atom depended only on its position relative to the other atoms and was calculated through the interatomic potential. The interatomic potential developed by Voter and Chen⁹ which used the embedded-atom method (EAM) was employed. It consisted of three pairwise potentials, which described the Ni-Ni, Al-Al, and Ni-Al interactions, and two embedding energies, which described the contribution to the energy of the electronic density around each type of atom. These functions were adjustable function which had been fitted with experimental results such as the lattice constants, the cohesive energy, vacancy energies, and so on. The cutoff distance of the interactions was between the fifth and sixth neighbors.

The simulations were performed on two different types of $\text{Ni}_{62.5}\text{Al}_{37.5}$ arrays, one ordered and one disordered, each containing 1024 atoms ($8 \times 8 \times 8$ bcc unit cell) with a lattice parameter of 2.88 Å. Stoichiometric Ni-Al has a *B2* structure: The atoms are ordered such that the corners of a cubic cell are occupied by Ni and the cell center by Al. The resulting simple cubic structure is therefore comprised of two distinct sublattices. In the case of $\text{Ni}_{62.5}\text{Al}_{37.5}$, nonstoichiometry is accommodated by Ni substitution on the Al sublattice without any other change in the type of cell. In what we will refer to as the disordered *B2* array, the "extra" Ni atoms were assigned at random [Fig. 1(a)] on the Al sublattice and in the bcc ordered supercell they were arranged in a regularly ordered pattern [Fig. 1(b)]. There are many ways of randomly distributing the "extra" Ni atoms on the Al sublattice, and to study the influence of this factor a run was performed at 10 K for 3000 steps (90 ps) for two configurationally different disordered *B2* arrays. To

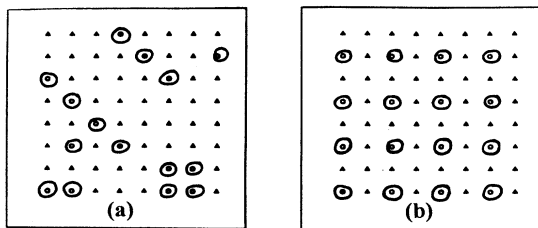


FIG. 1. One layer (from a total of eight layers) of the Al sublattice from the original arrays: (a) disordered *B2* array and (b) bcc ordered supercell. Circles represent Ni atoms, and triangles represent Al atoms; the extra Ni atoms on the Al sublattice are circled.

study the effect of supercell ordering, simulations were performed on both the disordered and ordered types of arrays at the same temperatures and for the same number of steps. To observe the behavior of tweed with temperature, the simulations were performed at 10, 80, 100, 300, 600, and 1000 K for 3000 steps (90 ps). The evolution of tweed versus time was studied in some detail by pursuing one run at 10 K for 12 000 steps (360 ps). Detailed examinations were made at the early stages of the simulation where diffraction patterns were calculated every 10 steps from step 10 (0.3 ps) to step 200 (6 ps). To analyze the static and dynamic components of tweed, the structure obtained after equilibrating the disordered *B2* array for 3000 steps at 10 K was heated in stepwise fashion to 100 K for 1000 steps (30 ps), then to 300 K for another 1000 steps, and finally to 600 K for 1000 more steps.

III. DATA ANALYSIS

In order to display the positions of the atoms clearly, the lattice was sliced into layers along a chosen orientation for purposes of plotting. The displacement of each atom relative to some chosen previous configuration was represented by a line (referred to as a "tail") joining the current position to the earlier position. Variants of this kind of drawing were used to represent the forces (or the strain gradient or strain) which acted on each atom by a tail pointing in the direction of the force (or the strain gradient or strain) and with the tail length proportional to the magnitude of the displayed quantity. One may also have the computer draw bonds between atoms whose interatomic distances lie in a chosen range for the purpose of locating new types of coordination that may develop.

Since the standard method for identifying tweed is based upon observing its characteristic diffuse diffraction pattern, a computer program was used to calculate diffraction patterns from the basic formula

$$I(k) = \sum_n f_n \exp(-i\mathbf{k} \cdot \mathbf{r}_n), \quad (1)$$

where I is the diffracted intensity, f_n is the scattering factor of atom n , \mathbf{k} is the wave vector, and \mathbf{r}_n is the position of atom n . The scattering factor of nickel has been taken as 6.8 Å, and the one for aluminum as 6.1 Å from values found by Hirsch *et al.*¹⁰ for forward scattering. The summation was performed over all particles in the array at a given time step.

IV. RESULTS AND DISCUSSION

A. Tweed pattern

The tweed diffraction pattern was observed with the disordered *B2* array at all temperatures studied, but it also showed significant variations with temperature. In the reciprocal lattice, the tweed pattern showed up as diffuse streaking along $\langle 110 \rangle^*$ directions. For the diffraction plots on $\{100\}^*$ planes, there were two possible variants for the streaking: one along the $[110]^*$ direction and one along the $[1-10]^*$, depending upon which Bragg peak was involved. At 10 K [Fig. 2(a)] a

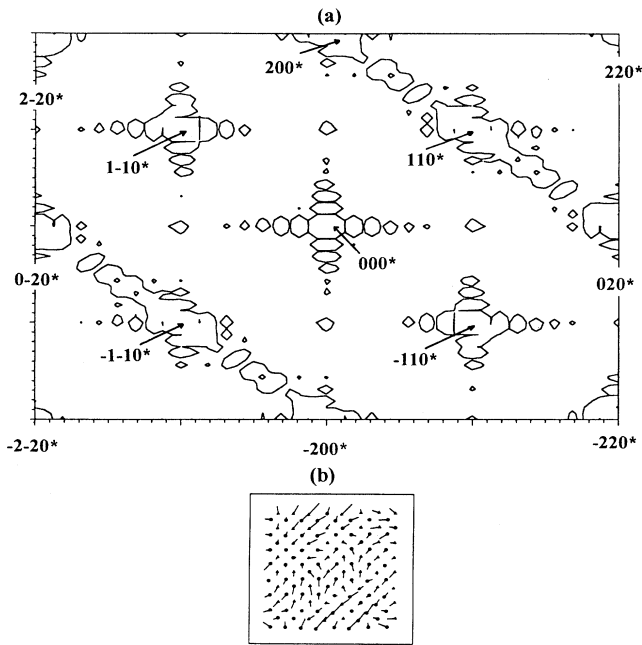


FIG. 2. Correspondence between atomic displacements and diffraction pattern at 10 K. Disordered $B2$ array at step 3000: (a) $(001)^*$ reciprocal plane and (b) atomic displacements ($4\times$ magnification) of one layer. Circles represent Ni; triangles represent Al atoms. In (a) the streaking along $\langle 100 \rangle^*$ is an artifact of our simulation box.

very strong streaking along one of the variant directions was visible which could be related to the $\{110\}\langle 1-10 \rangle$ shear occurring in the atomic displacement plots [Fig. 2(b)]. At 600 K a weaker diffuse streaking was observed along the two possible variants, and the displacement plots were more difficult to interpret because of the simultaneous activation of both variants of $\{110\}\langle 1-10 \rangle$ shears (Fig. 3). The variants activated (streaking along $[110]^*$ versus streaking along $[1-10]^*$) were found to depend upon the temperature, time, and starting configuration (Fig. 4).

At low temperature (10 K) a very strong streaking was also observed along the $[112]^*$ direction on the $(-110)^*$ plane (Fig. 5). No other equivalent direction (on other reciprocal planes) showed such a streaking. As the temperature increased, the $[112]^*$ streaking became weaker more rapidly than the $\langle 110 \rangle^*$ type of streaking. On the atomic plots, it was found that each of the $\{11-1\}$ rows was moving as a unit along the $[11-1]$ direction (Fig. 6). Honjo, Kodera, and Kitamura¹¹ suggested such a linear-chain motion for a number of metallic and nonmetallic materials based on observed diffraction patterns. This type of coordinated motion of rows which produced the $[112]^*$ streaking can also contribute to the $\langle 110 \rangle^*$ streaking as was demonstrated by the work of Otsuka, Wayman, and Kubo,⁷ who observed the same phenomenon in the case of Cu-Al-Ni and Cu-Zn.

The radial distribution function (histogram of the interparticle distance) of the structure obtained at 10 K after 3000 steps (90 ps) for the disordered $B2$ array exhib-

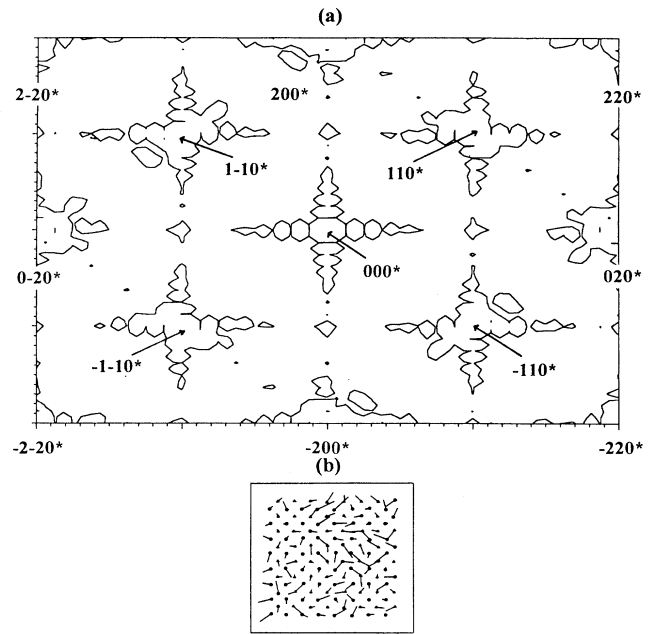


FIG. 3. Correspondence between atomic displacements and diffraction pattern at 600 K. Disordered $B2$ array at step 2000: (a) $(001)^*$ reciprocal plane and (b) atomic displacements ($4\times$ magnification) of one layer. Circles represent Ni; triangles represents Al atoms.

ited an extra peak situated between the second and third nearest-neighbor distances of the bcc lattice (Fig. 7). By plotting bonds between atoms whose interatomic distances were situated around the extra peak ($1.18a_0$, $a_0=2.88 \text{ \AA}$), we were able to discern connected regions in the lattice (Fig. 8). In these regions it was the second nearest-neighbor distance which had become larger. The plot exhibited two kinds of regions: one where the bonds reconnected in a zigzag pattern and the other where the bonds formed a parallel arrangement.

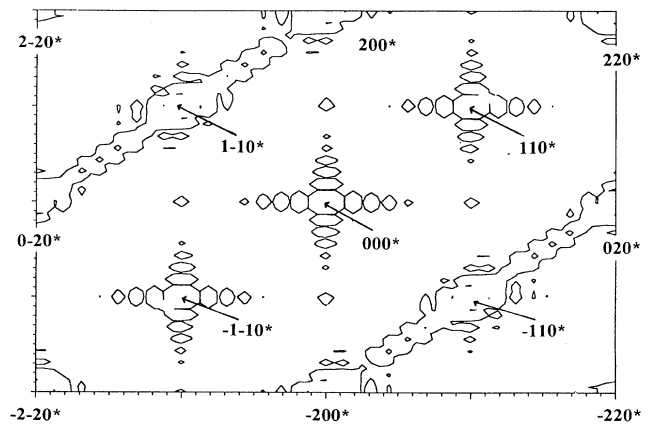


FIG. 4. Comparison between the two "disordered" $B2$ lattices. Diffraction pattern at 10 K for 3000 $(001)^*$ reciprocal plane: lattice 2 [to be compared with Fig. 2(a)].

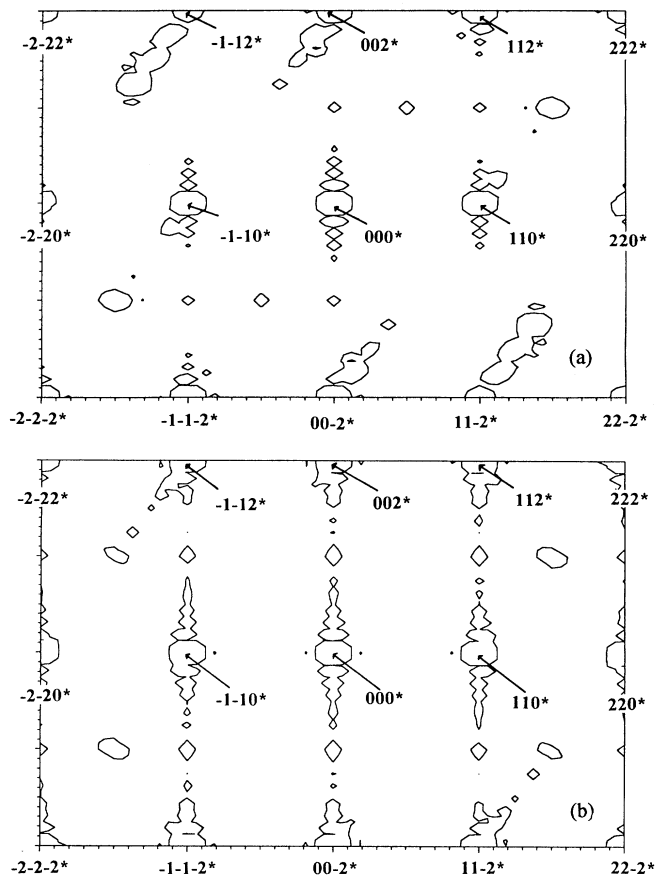


FIG. 5. Diffraction pattern of the $(1-10)^*$ reciprocal plane for the disordered $B2$ array at step 3000: (a) 10 K and (b) 80 K.

By plotting the strain gradient at each atom, these two kinds of regions could be further understood (Fig. 9). In the first kind, the strain gradient alternated in direction and magnitude, which is what a single $\{110\}\langle 1-10\rangle$ shear variant would show. In the second kind, the strain gradient alternated in direction from one row to the adjacent row and may be analyzed as a simultaneous double-shear

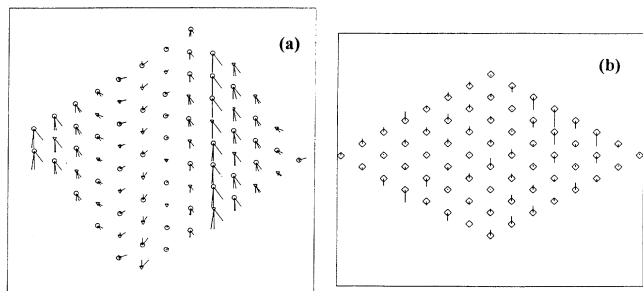


FIG. 6. Atomic plot of the disordered $B2$ array at 10 K for step 3000: (a) displacements ($2\times$ magnification) of one layer and projection of those displacements on $\langle 11-1\rangle$ and $\langle 110\rangle$ and (b) projection of the average displacements of the $\langle 11-1\rangle$ rows on $\langle 11-1\rangle$. Each diamond represents a $\langle 11-1\rangle$ row seen on end; the tail represents the average displacement of that row along the $\langle 11-1\rangle$ direction.

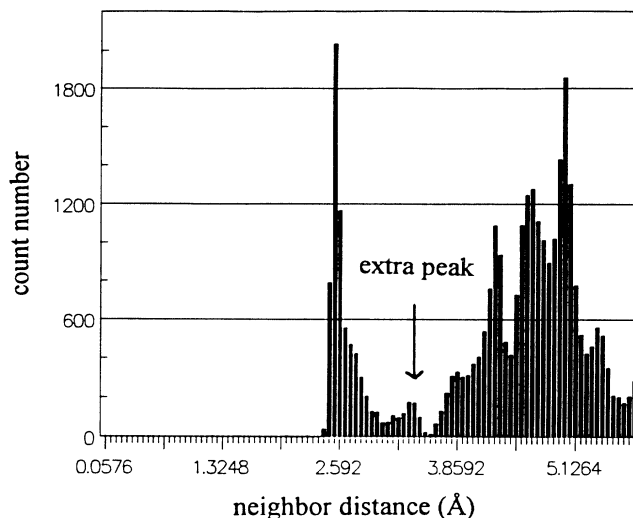


FIG. 7. Radial distribution function after 3000 steps at 10 K. Disordered $B2$ array. The small dots under the diagram indicate the positions of the neighbors in the ideal bcc lattice.

region. This type of double shear is equivalent to a tetragonal Bain strain as shown by Bogers and Burgers.¹² It is interesting to note that the “extra” Ni atoms did not show any strain gradient and seemed to act as centers of distortion in the lattice. A plot of the forces at step 0 showed that the “extra” Ni atoms were attracting all their neighbors and that three were nearly no net forces acting upon them (Fig. 10).

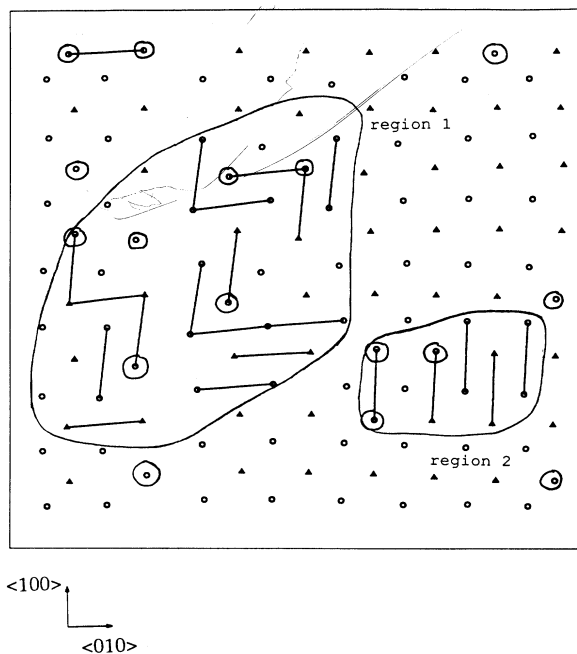


FIG. 8. Regions corresponding to the extra peak observed in the radial distribution function. Disordered $B2$ array. Circles represent Ni atoms; triangles represent Al atoms. Bonds are drawn between atoms whose distances are in the range $1.16a_0-1.20a_0$. The two types of regions have been circled.

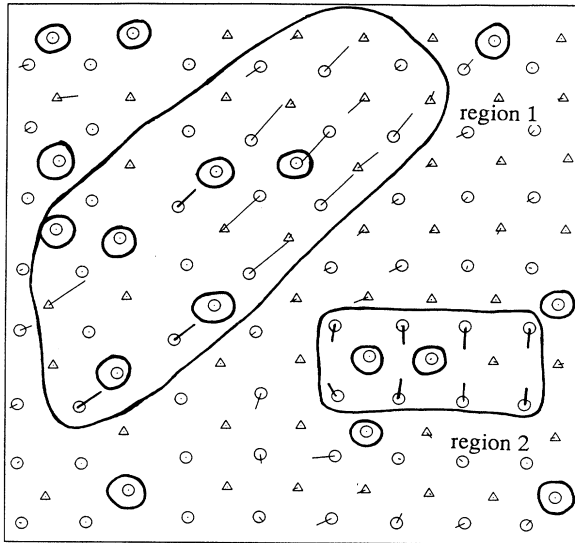


FIG. 9. Strain gradient pattern of 3000 steps at 10 K. Disordered $B2$ array. Circles represent Ni atoms; triangles represent Al atoms. The circled regions represent the two types of tweed regions.

B. Temperature dependence of tweed

From the diffraction patterns, it can be seen that the tweed pattern became more and more pronounced as the temperature decreased. To get more quantitative results, plots of the simulated diffraction intensity along $\langle 110 \rangle^*$

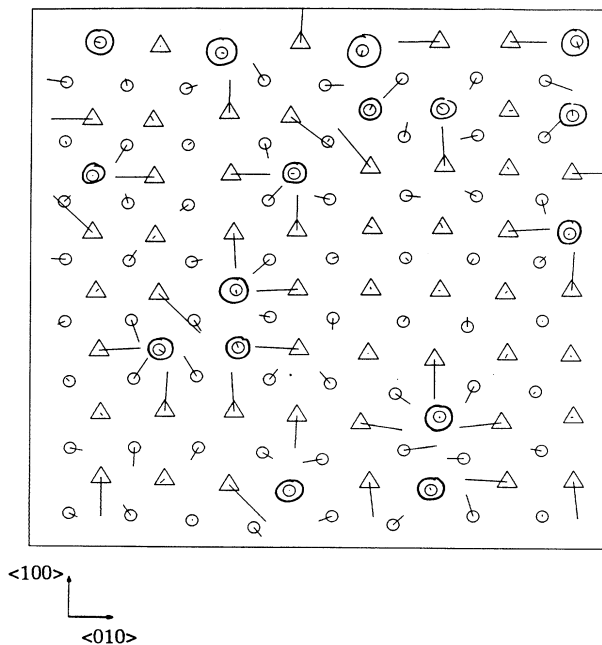


FIG. 10. Force pattern for step zero. Disordered $B2$ array. Circles represent Ni atoms; triangles represent Al atoms. The "extra" Ni atoms are circled in black.

directions were made for the plane $(001)^*$. To average out short-time fluctuations (which would be averaged out in experimental measurements), the intensity along the $[1-10]^*$ direction was added to the intensity along the $[110]^*$ direction and plotted (Fig. 11). This "average tweed intensity" decreased as the temperature increased, in agreement with experimental results.¹

C. Time sequence

The first anomalies in the 10-K diffraction pattern appeared at step 50 (1.5 ps). Very weak diffuse streaking developed along the two variants until step 500 (15 ps) when one variant ceased to develop. At 12 000 steps (360 ps), the diffraction pattern resembled very much the one obtained after only 3000 steps (90 ps) with only one very strong variant activated.

By successively increasing the temperature of the disordered $B2$ array (initially equilibrated at 10 K), the tweed pattern decreased in intensity as the temperature

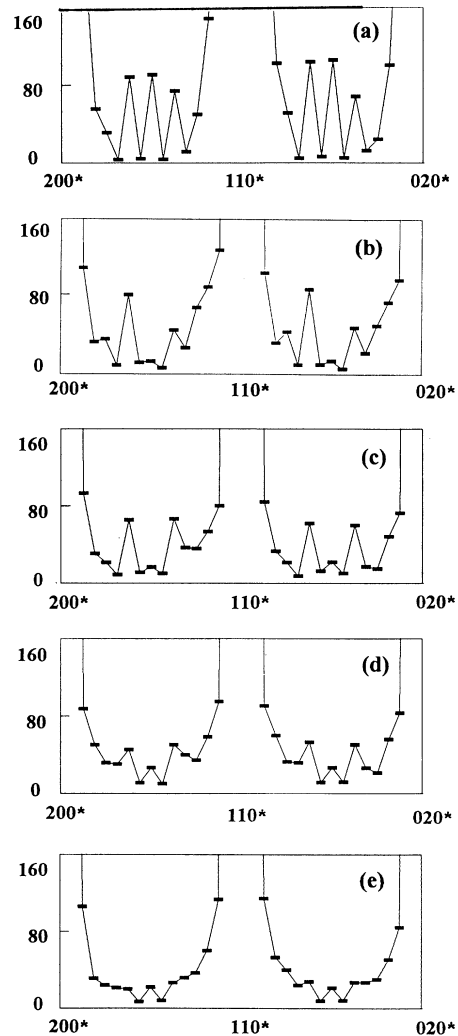


FIG. 11. Scan of the diffracted intensity along the $\langle 110 \rangle$ directions after 3000 equilibration steps. Disordered $B2$ array: (a) 10 K, (b) 80 K, (c) 100 K, (d) 300 K, and (e) 600 K.

increased; however, the number of variants activated increased. At low temperatures (10 and 80 K), the shear regions did not fluctuate appreciably between different variants. Apparently, the lattice did not have enough thermal energy to activate all the variants or even to shift from one to another. As a result, static "islands" of sheared material became fixed in the lattice. As the temperature increased, more variants were activated. In essence, the tweed had become more dynamic in character even as it became weaker. This agrees with neutron-scattering experiments on $\text{Ni}_{62.5}\text{Al}_{37.5}$ (Ref. 13) wherein the magnitude of the measured "central peak" (which corresponds to elastic scattering due to static distortions) increased as the temperature decreased, while the amplitude of the dynamic peak (corresponding to fluctuating features) decreased.

By contrast, in the simulations with the bcc ordered supercell (Fig. 12), at low temperature there was no streaking along the $\langle 110 \rangle^*$ direction and no evidence of $\{110\}\langle 1-10 \rangle$ shear in the displacement plots. There was also no $\langle 112 \rangle^*$ streaking and no coordinated motion of rows. As the temperature increased, only a very weak diffuse $\langle 110 \rangle^*$ streaking appeared, but there was still no appearance of $\{110\}\langle 1-10 \rangle$ shear in the displacement plots. Since the only difference between these simulations and those of the disordered arrays was the lack of compositional disorder, one may infer that compositional disorder (or some similar type of point strain centers, vacancies, interstitials, etc.) is necessary for "tweed" to appear, and it seems to show that tweed requires heterogeneous defects.

D. ω -phase instabilities

Our results are in good agreement with those of Otsuka, Wayman, and Kubo.⁷ Based on their diffraction patterns, they found that the $\langle 110 \rangle^*$ streakings they observed were too strong to be just interpreted as the result of the intersection of $\{111\}^*$ reciprocal-space walls with the Ewald sphere and that there also had to be $\langle 110 \rangle^*$ reciprocal-space rods superimposed on the $\{111\}^*$ reciprocal-space walls. Honjo, Kodera, and Kitamura¹¹

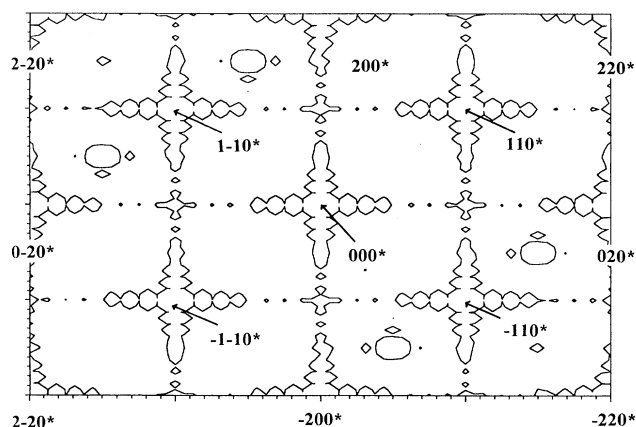


FIG. 12. Ordered supercell bcc lattice at 10 and 300 K for step 3000: (a) 10 K, $(001)^*$ reciprocal plane, and (b) 300 K, $(010)^*$ reciprocal plane.

suggested that the reciprocal-space walls were produced by linear-chain motions where rows of atoms in the close-packed directions move as units independently from each other. This was what was observed in our simulations at low temperature resulting from the motion of $[111]$ rows leading to the appearance of the $\langle 112 \rangle^*$ streaking in the diffraction pattern. Thus we found at low temperature strong static displacements of the $[111]$ rows superimposed on $\{110\}\langle 1-10 \rangle$ shear. Georgopoulos and Cohen¹⁴ have reported x-ray-scattering studies of the Ni-Al β phase in which they found diffuse-scattering patterns similar to that exhibited by the diffuse ω state in Ti and Zr alloys. They showed that the characteristic diffuse scattering was strongest away from stoichiometry in $\text{Ni}_{1-x}\text{Al}_{1-x}$ and proposed that the phase was heterogeneously nucleated by (111) planar collapse around point defects, such as the extra Ni atoms on the Al sublattice. Although we have looked carefully for such planar collapse in the atomic displacement computer plots, it was not evident and the reason for this may be that computer simulation displays ω instability at much earlier times than that of the x-ray experiments.

As a result, we speculate that the static $\{111\}$ row displacements may be the true initial precursors to the ω -phase transformation in this system. This is not a new idea, but very similar to one proposed by de Fontaine and Buck¹⁵ in modeling the β to ω transformation in Ti, Zr, and Hf alloys. The only basic difference between their model and ours is in the postulated source of the static row displacements. They imagined that the anharmonic potential for rigid row motion would have a triple-minimum character, with positive or negative displacements of $\frac{1}{3}$, the β nearest-neighbor distance having a somewhat deeper minimum than the minimum for no displacement. In fact, this potential can be calculated in our example and is displayed in Fig. 13, where it is evident that it has only a single minimum. Even so, their model remains of value here because they went on to show by means of a Monte Carlo simulation with assumed interactions between the adjacent rows that below some transition temperature neighboring rows would coordinate their displacements to form finite regions of the ω phase.

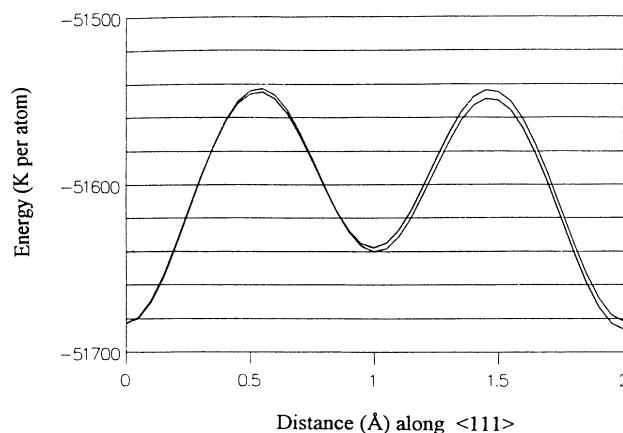


FIG. 13. Anharmonic potential for rigid row motion along $[111]$: The potentials for two different rows are represented.

By contrast, we believe that the driving force arises from a reduction of the local strain of the substitutional defects and thus is spatially heterogeneous, linked as it is to the defect positions at any moment. Since in the β phase the extra Ni atoms act as centers of dilatation on the Al sublattice and would have Ni atoms as their immediate nearest neighbors lying in $\langle 111 \rangle$ directions, this would be the direction of maximum compression. Because the elastic resistance to $\langle 111 \rangle$ row motion can be shown to be proportional to C' ($C_{11} - C_{12}/2$), which is anomalously low in the β Ni-Al phase (as in many other β phases showing similar phase instabilities), the expected displacement along these directions outward from a given extra Ni atom will be large. If a pair of extra Ni atoms occurs in close proximity on one particular $\langle 111 \rangle$ row, this could be thought of as forming a "strain dipole," producing unusually large displacements in the row forming its axis. It may be expected that strain dipoles would repel each other if their axes intersected, thus providing a tendency toward local alignment achieved by strain-driven diffusion and resulting in spatial-domain formation of each of the four possible $\langle 111 \rangle$ variants. If, in one domain, the row displacements alternated in magnitude in roughly the pattern shown in Fig. 14(a), as observed by de Fontaine and Buck, this would produce displacements equivalent to the (111) planar collapse picture, as indicated in Fig. 14(b). We imagine that this configuration would have the lowest strain energy of all, except for the case when one domain had grown to consume all the others.

Some direct support for this general model can be obtained from the high-resolution electron-microscopy observations of the ω phase in Ti-Mo alloys by Schryvers and Tanner,¹⁶ who have observed "linear structural arrays of < 1.5 nm length in $\langle 111 \rangle$ directions." At longer annealing times, these linear arrays begin to coalesce into two-dimensional (2D) regions which display clearer diffraction characteristics of the ω phase. They are unable to resolve their linear arrays sufficiently to determine

if they consist of just single $\langle 111 \rangle$ atomic rows or represent several adjacent rows,¹⁷ but in any case their observations would appear to prove that the first stage of ω -phase formation involves linear, and not planar, embryos.

This model would then also explain why long annealing times are generally necessary to develop ω -phase states in alloys, since the complicated diffusion process eventually leading to a coherent alignment of strain dipoles can be expected to be slow. In addition, it would clarify why an "incommensurate" ω state usually appears prior to the "commensurate" ω in many observed cases. It may also provide a basis for understanding the range of stoichiometry over which the ω instability will occur, given the expectation that some minimum concentration of defects will be necessary to lead to a cooperative ordering of strain dipoles, but also beyond some maximum concentration of defects, too much interference will occur to allow coherent alignments to grow.

Other linear $\langle 111 \rangle$ embryo models have been proposed in the past for the ω phase by Kuan and Sass.^{18,19} The main difference between those models and the one proposed here is that they assumed that the $\langle 111 \rangle$ atomic displacements are induced by a vacancy; there is no role for diffusion and strain field interaction, and they provide no explanation as to why the cubic symmetry around a single vacancy should be disturbed along only one of the four equivalent directions. Our explanation for the breaking of symmetry is that two substitutional defects in close proximity along one particular $\langle 111 \rangle$ row are required to set up the linear displacement field. We expect diffusion of this strain dipole as a bound entity interacting with other strain dipoles in its vicinity to be an essential part of the ω -phase ripening process. Although we may speculate that one of the substitutional defects could be a vacancy in forming the strain dipole, we have not carried out any extensive investigation of this possibility in our simulations.

Of course, we are also assuming that the substitutional binary defect model being proposed here is valid in general for the other bcc solid solutions in which ω -phase phenomena are observed, such as Zr-Nb, Ti-Mo, etc. It is interesting to note that both Nb and Mo substituting in Zr-rich and Ti-rich alloys, respectively, are smaller than their host atoms judged by the decrease in lattice parameter with increasing substitution and therefore in this respect would generate the same kinds of strain as excess Ni on the Al sublattice in Ni-Al.

There are also some interesting links between the soliton model put forward by Horovitz, Murray, and Krumhansl²⁰ and the strain dipole model outlined here. To quote from their paper, "Thus we assume that the ω clusters are one-dimensional objects which interact with the surrounding β matrix," and later, "We study a model 1D chain with a natural lattice parameter $a-d$ nucleated in a matrix with a lattice parameter. This is similar to a 1D epitaxy problem." It is this frustration between the 1D ω cluster "natural spacing" and that of the parent β matrix which they argue will lead to solitons once the mismatch is greater than some critical value. They however never specify the atomic nature or composition of

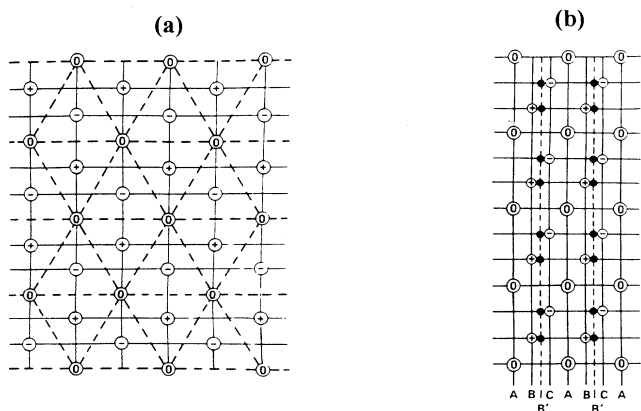


FIG. 14. Formation of the ω phase: (a) projection of β structure on (111) plane. Minus signs represent atoms below the plane of projection, plus signs represent atoms above the plane of projection, and O's represent atoms in plane of projection. (b) Schematic collapse of the atoms leading to the formation of the ω phase. From Ref. 15.

their 1D chains and in fact treat the alloy as completely random solid solution, since they say "... we consider the smaller Nb atoms as the source of the pressure term... We assume that the randomly distributed Nb atoms lead to a homogeneous pressure which implies that the ω cluster tends to have a smaller lattice constant."

We would also argue that 1D chains are the basic structural unit, but here we have provided their explicit atomic and compositional character which we claim occurs only as a result of the nonrandom solute distribution. Indeed, we would agree it is the size disparity which sets up the local strain (or "frustration"), but it is their ability to lower their strain energy by diffusing into adjacent offset parallel positions that allows 3D ω clusters to form.

V. CONCLUSIONS

Using EAM interactions for the Ni-Al alloy system, molecular-dynamics simulations of $\text{Ni}_{62.5}\text{Al}_{37.5}$ arrays containing 1024 atoms showed tweed phenomena under a variety of conditions similar to that which has been reported experimentally. Tweed structure in the simulations only occurred if compositional or crystalline defects were in the lattice. The most important defect appeared to be random Ni atoms on Al sites. From this we conclude that heterogeneities were necessary (at least in this system) to produce tweed structure. Tweed structure in the simulations increased in intensity with decreasing temperature in agreement with experiment. The tweed

structure was primarily static at low temperature, but primarily dynamic at higher temperatures, in agreement with indications from neutron-scattering data. Thus the two theories (dynamic versus static) are each valid, but in different temperature domains. Two types of "tweed regions" were found in the static case: (a) single (110) shear regions and (b) Bain strain regions.

We also found that $\langle 111 \rangle$ row displacements initiated by Ni substitutional defects at low temperature produced $\langle 112 \rangle^*$ diffuse streaking in the diffraction pattern, analogous to that observed when incommensurate the ω phase is said to be present in an alloy. We suggested that these static row displacements (representing strain dipoles) are the very first stage of ω -phase formation and speculated that subsequent stages involve diffusion of the substitutional defects to reduce the strain field interaction energy between these dipoles, ultimately leading to the ordered pattern recognizable as a "commensurate ω phase."

In our simulations, although both tweed and ω -type diffuse scattering was formed (as is also shown by experiments), as the temperature was increased the tweed $\{110\}\langle 1-10 \rangle$ shear became more dynamic and tended to suppress or average out the ω -like $\langle 111 \rangle$ row displacements.

ACKNOWLEDGMENTS

We would like to thank L. E. Tanner for his help and constructive comments about this work. This research was made possible by a grant from the U.S. Department of Energy and from the Lawrence Livermore National Laboratory.

¹L. E. Tanner, *Philos. Mag.* **14**, 111 (1966).

²S. M. Shapiro, B. X. Yang, Y. Noda, L. E. Tanner, and D. Schryvers, *Phys. Rev. B* **44**, 9301 (1991).

³N. Rusovic and H. Warlimont, *Phys. Status Solidi A* **44**, 609 (1977).

⁴S. M. Shapiro, J. Z. Larese, Y. Noda, S. C. Moss, and L. E. Tanner, *Phys. Rev. Lett.* **57**, 3199 (1986).

⁵I. M. Robertson and C. M. Wayman, *Philos. Mag. A* **48**, 421 (1983).

⁶Z. H. Kalman, L. H. Lee, X. C. He, and S. Weissmann, *Metall. Trans. A* **19**, 217 (1988).

⁷K. Otsuka, C. M. Wayman, and H. Kubo, *Metall. Trans. A* **9**, 1075 (1978).

⁸A. Silberstein and P. C. Clapp, *Phys. Rev. B* **38**, 9555 (1988).

⁹A. F. Voter and S. P. Chen, in *Characterization of Defects in Materials*, edited by R. W. Siegal, J. R. Weertman, and R. Sinclair, *Mater. Res. Soc. Symp. Proc. No. 82* (Materials Research Society, Pittsburgh, 1987), p. 175.

¹⁰P. Hirsch, A. Howie, R. B. Nicholson, D. W. Pashley, and M. J. Whelan, *Electron Microscopy of Thin Crystals* (Krieger, Malabar, 1977), pp. 504–505.

¹¹G. Honjo, S. Koderia, and N. Kitamura, *J. Phys. Soc. Jpn.* **19**, 351 (1964).

¹²A. J. Bogers and W. M. Burgers, *Acta Metall.* **12**, 255 (1964).

¹³L. E. Tanner, S. M. Shapiro, D. Schryvers, and Y. Noda, *Mater. Res. Soc. Symp. Proc.* **246**, 265 (1992).

¹⁴P. Georgopoulos and J. B. Cohen, *Acta Metall.* **29**, 1535 (1981).

¹⁵D. de Fontaine and O. Buck, *Philos. Mag.* **27**, 967 (1973).

¹⁶D. Schryvers and L. E. Tanner, *Mater. Sci. Forum* **56-58**, 329 (1990).

¹⁷L. E. Tanner (private communication).

¹⁸T. S. Kuan and S. L. Sass, *Acta Metall.* **24**, 1053 (1976).

¹⁹T. S. Kuan and S. L. Sass, *Philos. Mag.* **36**, 1473 (1977).

²⁰B. Horovitz, J. L. Murray, and J. A. Krumhansl, *Phys. Rev. B* **18**, 3549 (1978).